Preliminary Design for a Thermionic R.F. - Gun*

G. D'Auria, J. Gonichon, T. Manfroi**
Sincrotrone Trieste
Padriciano 99, Trieste, Italy

Abstract

A high-gradient S-band RF-Gun with a thermionic LaB_6 cathode is now under study at Sincrotrone Trieste for future upgrading of the injection Linac. A geometry of the accelerating structure has been designed using the OSCAR2D code and a prototype has been constructed and measured. The transverse and longitudinal dynamics of the particles along the injector have been simulated with a modified version of the PARMELA code.

I. INTRODUCTION

The proper functioning of the injection system is of fundamental importance in order to have both high current and small emittances. Electron guns, however, have intrinsic limitations when combined with conventional R.F. systems (choppers-bunchers). In the last years special care has been devoted to R.F. gun development which promises to be a solution to these limitations with the production of very bright beams.

The system described here should be able to produce an electron beam for injection into a linac [1]; the beam characteristics should also fit the requirements for a FEL experiment, i.e. low emittance, low energy spread and high peak current. At injection into the Linac, the expected beam characteristics are summarized in table 1.

Table 1.

Average beam energy	1.1 MeV
Micropulse peak current	≥ 20 A
Transverse normalized emittance	≤ 20 π mm mrad
Relative energy spread	≤ 20%

The injector will consist of an RF cavity working in the fundamental mode at 3 GHz provided with a thermionic LaB_6 cathode, an alpha-magnet, and four quadrupoles which focus the beam into the alpha-magnet and the Linac.

II. DESCRIPTION OF THE INJECTOR

Figure 1 shows a schematic diagram of the injector. The RF cavity is powered by a 2.6 MW magnetron (EEV. mod. M5193) operating with a 3 μsec macropulse length at a maximum repetition rate of 100 Hz.

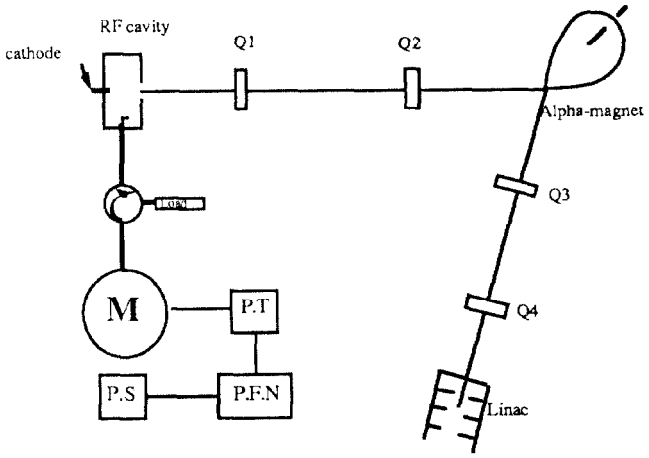

Figure 1. Injector layout.

A 5.2 MW line-type modulator supplies the negative H.V. pulse to the magnetron. The P.F.N. consists of 10 "lumped constant" L-C elements followed by a H.V. pulse transformer; the line is charged by a 20KV-0.1A D.C. power supply. A 3-port circulator is foreseen between the magnetron and the RF cavity. From the 2.6 MW delivered by the magnetron, only 1.8 MW can go to the beam due to the cavity losses and the feeding line attenuation. For an average beam kinetic energy of 1.1 MeV, this implies a maximum current of 1.63 A ($3.38 \cdot 10^9$ electrons per bunch for a 3 μsec pulse length). This current is produced by a 3 mm LaB_6 thermionic cathode heated to 1800-1900 K. The purpose of the alpha-magnet system [2] is to reduce the wide energy spread of the beam exiting the cavity and to compress the bunch. Electrons with different energies follow different alpha-shaped trajectories, allowing an energy range to be selected through the use of slits. Moreover, the more energetic electrons (emitted earlier) spend more time in the magnet than the less energetic ones (emitted later), resulting in a phase compression that can be adjusted by varying the magnetic field. Two quadrupoles are placed between the cavity and the alpha-magnet and two between the alpha-magnet and the Linac, allowing the matching of the beam into the alpha-magnet and the Linac, as well as the control of emittance.

III. CAVITY DESIGN AND MEASUREMENTS

The cavity design has been performed using the OSCAR2D code [3,4]. The geometry has been chosen in order to optimize the beam parameters at the cavity exit. The accelerating gradient along the beam axis has been maximized

* Work carried out in cooperation with the University of Trieste.
** Dipartimento di Fisica, Università di Trieste.

0-7803-0135-8/91$03.00 ©IEEE

to accelerate the particles in as short a time as possible, reducing the space charge effects in the low-γ region. The cavity profile is shown in figure 2; figure 3 shows the behaviour of the electric field components along the z-axis for three values of r. The nose geometries are different: an optimum shape has been found for the one nearest the cathode to maximize the E-field in that region and to break the cavity symmetry. Furthermore, the behaviour of the radial electric field is linear [5] as it is shown in figure 4.

A prototype of the cavity has been realized and measured to verify the electric parameters. Table 2 shows the computed and measured values.

Table 2.

	Computed	Measured
Resonant frequency (MHz)	3016.73	3004.907
Q value	12000	9000
R_{SH} (MΩ)	2	1.54
$E_{max.sup}/E_{max.axis}$	1.6	-

IV. DYNAMIC SIMULATIONS

A modified version of PARMELA [6,7] was used to simulate the transverse and longitudinal motion of the particles all along the system. The beam represented by a collection of macro-particles, each located at three spatial and three momentum coordinates, is transformed through the system via numerical integration of the equations of motion, using the phase of the RF field as the independent variable.

At the cathode, the particles are emitted between 0 and 180° (in half a cycle of 3 GHz) according to the Richardson-Schottky law (most of the particles are emitted when $\phi = 90°$, i.e. when the electric field at the cathode is maximum). The distribution of the initial momenta is gaussian, as well as the one for the transverse spatial coordinates.

Just after leaving the cathode, the particles experience the E_Z, E_r, and B_ϕ RF fields present in the cavity. About half the particles exit the cavity whereas the other return to hit the cathode. This back-bombardment has the effect of heating the cathode and impedes the maintainment of a constant current during the pulse duration. This problem could be solved by adding a transverse magnetic field near the cathode for a correct FEL operation. In the conditions of operation described in table 3, the average back-bombardment power was found to be 8.2 W (10 pps. for 3 μs pulse).

In the alpha-magnet, the equations of motion for each particle are solved for the position and the momenta in the alpha-magnet coordinates system, and then transformed to the injector coordinates [8]. The magnetic field, as well as the spacing between the two energy slits can be varied. The alpha-magnet further reduces the number of particles by one half, reducing in the same way the emittance and leaves roughly 20% of the total charge at the cathode going into the Linac.

A particle is considered lost when it touches the vacuum chamber wall or the energy slits in the alpha-magnet, or when its longitudinal velocity becomes lower than zero. The space charge forces are evaluated by a full 3 dimensions relativistic point by point calculation: the coulomb interaction between each macro-particles is calculated at every time step. Beam loading and wake field effects are not included in this simulation.

V. RESULTS

The system parameters used for the simulation are described in table 3.

Table 3.

0 cm	Cathode	R = 1.5 mm W = 0.5 eV T = 1900 °K Total charge = 0.5 nC
0-3.77 cm	Cavity	E_{zmax} = 63 MV/m $\bar{E}_z$ = 37 MV/m E_{zcat} = 30 MV/m
10.8-15.2 cm	Q1	G = 110 Gauss/cm
22.2-26.6 cm	Q2	G = -90 Gauss/cm
33.8-64.8 cm	Alpha-magnet	G = 140 Gauss/cm
71.8-76.2 cm	Q3	G = 25 Gauss/cm
83.2-87.6 cm	Q4	G = -50 Gauss/cm
93.8 cm	Linac	

Since the space charge calculations are very time consuming (CPU_{time} α (number of particle)^2), Parmela has been installed on a very powerful workstation: Hewlett-Packard 9000/834, risc architecture, 17 Mips. This enable us to simulate a single bunch with 300 "macro-particles" taking a computation time of 50 mn. The simulation presented here has been made with a thousand of "macro-particles" (9 h).

In what follows, all the emittances are normalized and defined in the rms sense.

Just after the cavity, it can be seen in figures 5 and 6 that the bunch extends over roughly 200° of phase with an energy varying from 0 to 1.2 MeV. The transverse emittance is less than 10 π mm. mrad. Between the cavity and the alpha-magnet, the bunch becomes wider in phase because of the large energy spread. For the same reason, the transverse emittance growth is very important.

Just after the alpha magnet, the number of particles drops to 225 (23% of the total), and the transverse emittance becomes 9.1 π mm. mrad. (5.6 π mm. mrad) in the x (y) plane. The energy lies between 0.98 and 1.2 MeV, and the phase extension is about 25°.

At the end of the injector (figures 8 and 9), i.e. just before the Linac, we obtain a bunch of roughly 7° long (6.5 ps), with a relative energy spread of 19%, and a transverse normalized emittance of 9.2 (7.6) π mm. mrad. in the x (y) plane. The remaining charge is 112 pC, leading to a peak current of 17 A.

This bunch has been further simulated through the two accelerating sections of the ELETTRA Linac [1]; at 98 MeV the transverse normalized emittance of the beam is 9.7 π mm. mrad. and 11.6 π mm. mrad. in x and y plane respectively. The relative energy spread has been reduced to ± 0.25%. We find 84 pC in 5° leading to a peak current of 18 A.

This peak current is below the expected characteristics, but could be increased by upgrading the power source.

VI. REFERENCES

[1] C. Bourat et al., "The 100 MeV Preinjector for the Trieste Synchrotron", EPAC 1988.

[2] H.A. Enge, "Achromatic Magnetic Mirror for Ion Beams", Rev. Sci. Instrum. BF 23, No. 4, 385-389 (1963).

[3] R. Parodi, P. Fernandes, "OSCAR2D User's Guide", Genoa, November 1989.

[4] T. Manfroi, "Studi su sorgenti di elettroni a bassa emittanza", Degree Thesis, Univ. Trieste, April 1991.

[5] M.E. Jones et al., "Particle-in-cell simulations of the lasertron", IEEE Trans. on Nucl. Sc., Vol. NS-32, No. 5.

[6] User's manual from B.Mouton LAL/SERA 89-356, 1989.

[7] H. Liu, "Particle Generation for Simulation of RF Thermoionic Guns", LAL/ SERA 90-178, June 1990.

[8] H. Liu, "Description about How to Input an Alpha Magnet Card in PARMELA", private communication.

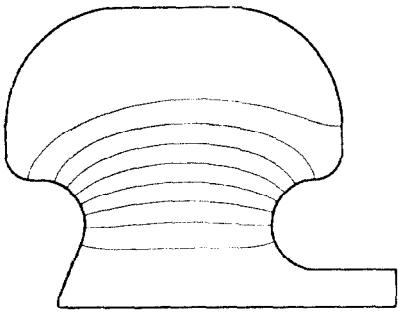

Figure 2. Cavity profile.

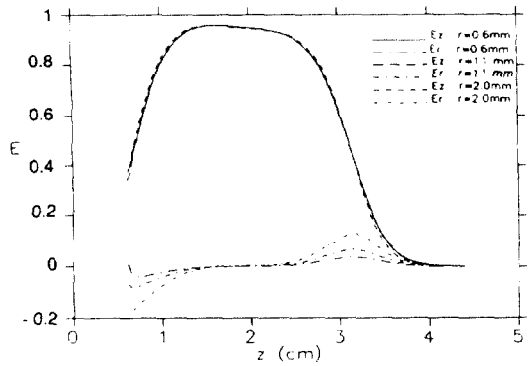

Figure 3. Relative amplitudes of E-field components.

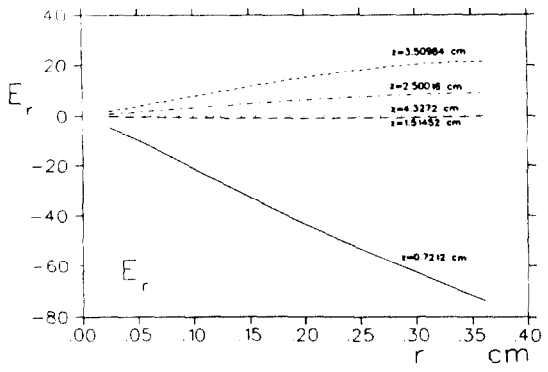

Figure 4. Radial electric field behaviour.

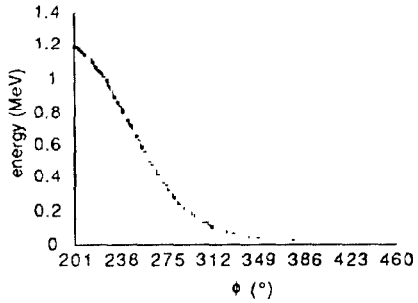

Figure 5. Longitudinal phase space after the cavity.

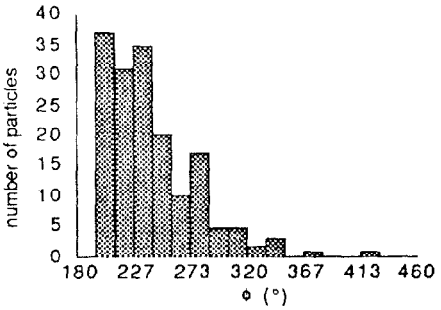

Figure 6. Phase distribution after the cavity.

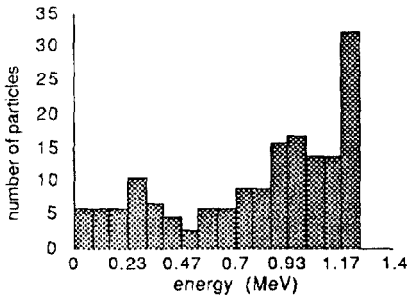

Figure 7. Energy distribution after the cavity.

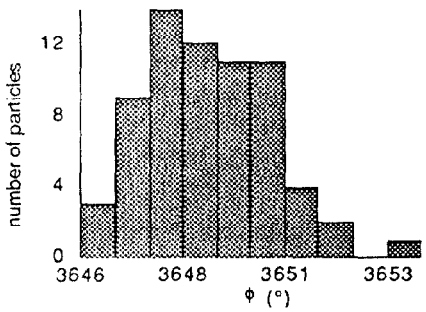

Figure 8. Phase distribution before the Linac.

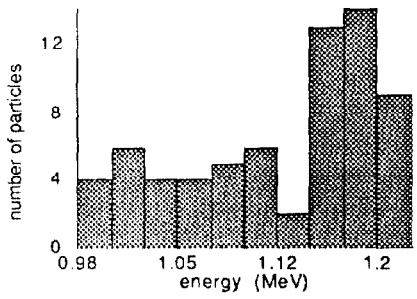

Figure 9. Energy distribution before the Linac.